2022

3D Conjugate Heat Transfer Modelling of E-Compressor

Abhishek Ballani

Mingyuan Tao

Chiranth Srinivasan

Haiyang Gao

Dipak Maiti

See next page for additional authors

Authors
Abhishek Ballani, Mingyuan Tao, Chiranth Srinivasan, Haiyang Gao, Dipak Maiti, and Sujan Dhar

3D Conjugate Heat Transfer Modelling of E-Compressor

Abhishek BALLANI [1], Mingyuan TAO[1], Chiranth SRINIVASAN[2*], Haiyang GAO[1], Dipak MAITI[1], Sujan DHAR[1]

[1]Simerics, Inc
[2*]Simerics, Inc, cs@simerics.com

ABSTRACT

E-Compressor has been widely used in the A/C systems of electric and hybrid vehicles due to advantages such as easy controllability and good efficiencies. In the present work, a 3-D thermal-fluid coupled methodology is devised using the commercial CFD software SimericsMP+® to investigate performance of an electric scroll compressor for different operating conditions. Gaseous refrigerant enters the system at low pressure and temperature condition, flows through the electric scroll compressor system, and exits at high pressure and temperature. Simulations were performed to study the effect of different tip leakage sizes ranging from 0 to 100 μm on the E-Compressor output. The volumetric efficiency of E-Compressor significantly decreases with large tip leakage size. The methodology was extended to couple the conjugate heat transfer physics to the Fluid Structure Interaction (FSI) of a reed valve downstream of the scroll compressor. It was noticed that the volumetric efficiency of scroll compressor does show major differences. The devised methodology is observed to be numerically robust and accurate, while achieving good computational efficiency.

1. INTRODUCTION

Scroll compressors are widely used in HVAC industries, in A/C systems or as superchargers of automobiles, and also as vacuum pumps. Due to fewer number of moving parts, scroll compressors are more reliable, and operate with low noise and vibrations compared to reciprocating compressors. Understanding the flow field is important when working on improving the performance of scroll compressors. There are several theoretical models to predict the performance of scroll compressors. Computational Fluid Dynamics (CFD) can be used to study the flow field and reduce several flow losses. But the challenges while performing CFD analysis of scroll compressors involve handling the mesh due to large deformation of the fluid volume between the fixed and orbiting scrolls and also the complicated leakage paths for the fluid. Gao and Jiang (2014) developed an automated template meshing strategy for generating and controlling the mesh for scroll compressors that is used in the present work. The details of the meshing strategy are explained in (Gao and Jiang, 2014, Gao et al., 2015). Using this method, Sun et al. (2017) performed 3D transient CFD analysis of a scroll compressor to understand the 3D flow and temperature field at different orbiting angles. Gao et al. (2015) used the same method to perform CFD simulations of a scroll compressor and predict the influence of a tip leakage seal.

With trends of electrification in the automotive industry, it is more and more common for the HVAC system components are driven by a small electric motor. The electric motor and the compressor, in fact, form a coupled system. While the electric motor forms the drive unit for the compressor, the gas being compressed serves as the coolant for the electric motor coil. This combined unit is colloquially known as an E-compressor. In the present work, 3D transient Conjugate Heat Transfer (CHT) simulation of a scroll type E-compressor using the commercial CFD tool, SimericsMP+® are performed in order to understand the influence of tip leakage gap on different performance parameters of the E-compressor. The solid side heat transfer analysis was included in order to understand the temperature distribution and its influence on the compressor performance. The method is extended to study the effect of including a reed valve at the discharge port of the scroll compressor using Fluid Structure Interaction (FSI).

2. Methodology

2.1 Fluid Solid Coupling

The present work deals with a coupled simulation of the fluid and solid sides of a scroll E-compressor assembly. The assembly includes an electrical motor side that includes the stator & rotor for the motor and a scroll compressor side that includes fixed & orbiting scrolls. The rotating parts are supported on a common shaft and some bearings. The complete assembly is placed inside an outer casing.

The operation of the E-compressor can be divided into two parts. In the first part, the refrigerant enters the E-compressor assembly at low temperature. This low temperature refrigerant passes through the motor and acts as a coolant to take up some heat. This results in rise in temperature of the refrigerant. In the second part, the refrigerant passes through the scroll compressor where it is compressed, and the fluid temperature increases further. This heat is then transferred to the solids of the scroll compressor and to other solid components through conduction. In order to accurately study the temperature distribution for the assembly, the fluid and heat equations need to be solved for both fluid and solid sides of the assembly.

As explained in (Dhar et al., 2019, Ding et al., 2019), the time taken to stabilize the flow and temperature fields on fluid side is only few cycles of the scroll compressor. But due to high thermal inertia, the solid side temperatures might take few minutes to stabilize. The computational time to simulate few minutes, i.e., thousands of cycles of the compressor, is not affordable. Hence, the fluid and solid side simulations are coupled by a Mixed Timescale Coupling approach. It follows an iterative approach where fluid and solid are solved separately while exchanging the temperature and heat flux data. Here, the fluid side simulation is performed as a transient simulation for one cycle of the scroll compressor where the temperature of the solids is used as boundary condition on the fluid-solid interfaces over the entire cycle. The solid simulation is then performed as a steady-state simulation where the heat flux from the fluid is used as boundary condition on the fluid-solid interfaces. Then the new solid temperatures are again transferred for the next fluid cycle simulation. This process is continued until a stable temperature distribution and heat balance between the fluid and solid side is achieved.

2.2 Governing Equations

A finite volume approach is used for the solution of the conservation equations of mass, momentum and energy. The conservations laws can be written as follows:

$$\frac{\partial}{\partial t}\int_{\Omega(t)} \rho d\Omega + \int_{\sigma} \rho(v - v_\sigma) \cdot n d\sigma = 0 \tag{1}$$

$$\frac{\partial}{\partial t}\int_{\Omega(t)} \rho v d\Omega + \int_{\sigma} \rho\big((v - v_\sigma) \cdot n\big) v d\sigma = \int_{\sigma} \tilde{\tau} \cdot n d\sigma - \int_{\sigma} P n d\sigma + \int_{\Omega} f d\Omega \tag{2}$$

$$\frac{\partial}{\partial t}\int_{\Omega(t)} \rho E d\Omega + \int_{\sigma} \rho\big((v - v_\sigma) \cdot n\big) E d\sigma = \int_{\sigma} k\nabla T \cdot n d\sigma - \int_{\sigma} p v \cdot n d\sigma + \int_{\sigma} (v \cdot \tilde{\tau}) \cdot n d\sigma + \int_{\Omega} f \cdot v d\Omega \tag{3}$$

For the solid model, only the energy equation is solved. To account for turbulence in the fluid model, the standard $k - \varepsilon$ two-equation model with wall functions is used that can be expressed as follows:

$$\frac{\partial}{\partial t}\int_{\Omega(t)} \rho k d\Omega + \int_{\sigma} \rho\big((v - v_\sigma) \cdot n\big) k d\sigma = \int_{\sigma} \left(\mu + \frac{\mu_t}{\sigma_k}\right) (\nabla \mathrm{k} \cdot n) d\sigma + \int_{\Omega} (G_t - \rho\epsilon) d\Omega \tag{4}$$

$$\frac{\partial}{\partial t}\int_{\Omega(t)} \rho \varepsilon d\Omega + \int_{\sigma} \rho\big((v - v_\sigma) \cdot n\big) \varepsilon d\sigma = \int_{\sigma} \left(\mu + \frac{\mu_t}{\sigma_\varepsilon}\right) (\nabla \epsilon \cdot n) d\sigma + \int_{\Omega} \left(c_1 G_t \frac{\varepsilon}{k} - c_2 \rho \frac{\varepsilon^2}{k}\right) d\Omega \tag{5}$$

2.3 Fluid Model

The fluid domain is extracted using standard CAD operations commonly available in any CAD package. The extracted fluid domain was then split into few parts in order to assign the rotation conditions to the required regions like the motor rotor, bearings, etc. The fluid domain is meshed using the General Mesher available in SimericsMP+® except for the scroll and reed valve. The General Mesher uses an automated binary tree meshing algorithm. It starts by splitting the domain into Cartesian hexahedral cells and refines the cell sizes by a factor of two near the boundaries in order to accurately capture the surfaces. The advantages of binary tree meshing are highlighted in Ding et al. (2011).

The deforming region of the scroll compressor is split and the split CAD is used to generate the mesh of scroll compressor. As shown in Figure 1, structured hexahedral mesh is generated in scroll region. The mesh deformation upon rotation of the orbiting scroll is handled by the scroll template during simulation.

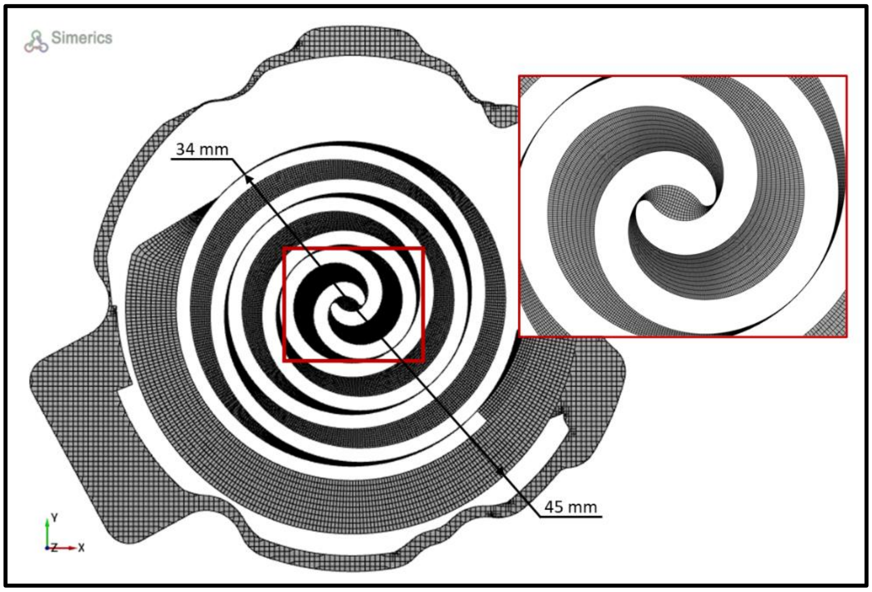

Figure 1: Cross-section view of scroll rotor template mesh.

The cross-section view of the Reed valve mesh at two different positions of the valve is shown in Figure 2. The opening of the reed valve is controlled by Fluid Structure Interaction approach where the following torsional dynamics equation is solved for angular displacement of the valve against the fluid torque acting on the valve. More details about the modelling a reed valve are described in Ding and Gao (2014).

$$I\frac{d^2\theta}{dt^2} + C\frac{d\theta}{dt} + k\theta = \tau(t) \tag{6}$$

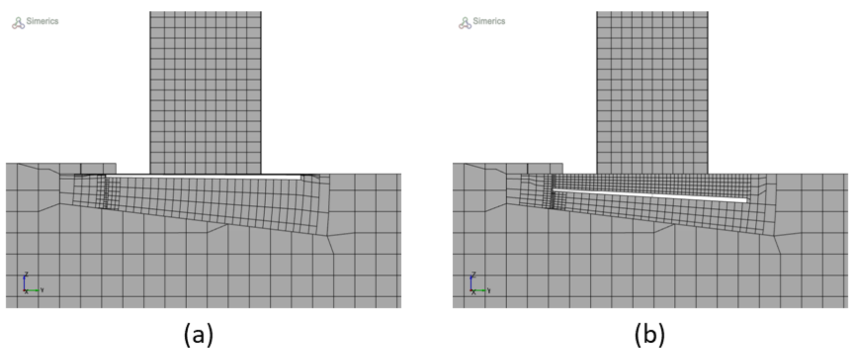

Figure 2: Cross-section view of reed valve mesh at (a) closed position and (b) 5° opening

The specifications of the scroll compressor are shown in Table 1.

Table 1. Scroll Compressor specifications

Items	Specifications
Suction Volume $[mL]$	15.4
Scroll Height $[mm]$	19.4
Scroll Thickness $[mm]$	2.89
Suction Temperature $[°C]$	12
Suction Pressure $[bar]$	3
Discharge Pressure $[bar]$	11
Radial Clearance $[\mu m]$	20

The working fluid is R1234yf in its gaseous form. The properties of the refrigerant like density, viscosity, conductivity etc. are provided as a function of temperature and pressure from NIST tables (Lemmon et al., 2007). The suction pressure and temperature for the fluid is set to 3 bar and 12 °C while the discharge pressure is fixed to 11 bar. The motor and the scroll are rotating at 8600 rpm. The fluid solid interface boundaries are assigned as temperature boundary condition from the solid side simulation which is mapped using the Mixed Timescale Coupling approach.

2.4 Solid Model

The solid mesh is generated using the General Mesher in SimericsMP+®. All solid components of the assembly including motor, bearings, scroll and casing are included in the simulation. Total mesh count of the solid model is around 3 million.

The motor coil, stator and rotor are assigned a total heat source of 108 W, 75.6 W and 32.4 W respectively. The fluid-solid interface boundaries are assigned convection boundary condition where the heat transfer coefficient and the fluid reference temperature are mapped from the fluid side by the Mixed Timescale Coupling approach. The remaining boundaries open to atmosphere are assigned convection boundary condition with heat transfer coefficient of 5 W/m^2K and ambient temperature of 15 °C.

3. Results and Discussion

3.1 Mesh Independent Study

Two cases with different mesh size were compared to ensure the mesh independence. For mesh 1, the maximum cell size is 1 mm; For mesh 2, the maximum cell size is reduced to 0.5 mm. Total cell count is 1.7 million for mesh 1 and 5.9 million for mesh 2. Figure 3 and Figure 4 show the comparison of mass flow rate and average temperature at outlet boundary. The revolution-averaged mass flow rate is around 119 kg/hour for both cases. The average temperature on outlet boundary is around 48.2 ℃ for both cases as shown in Figure 4. Mesh 1 with coarse mesh performs close enough flow and thermal properties as mesh 2 with fine mesh. Therefore, the mesh settings of mesh 1 is adopted in this work.

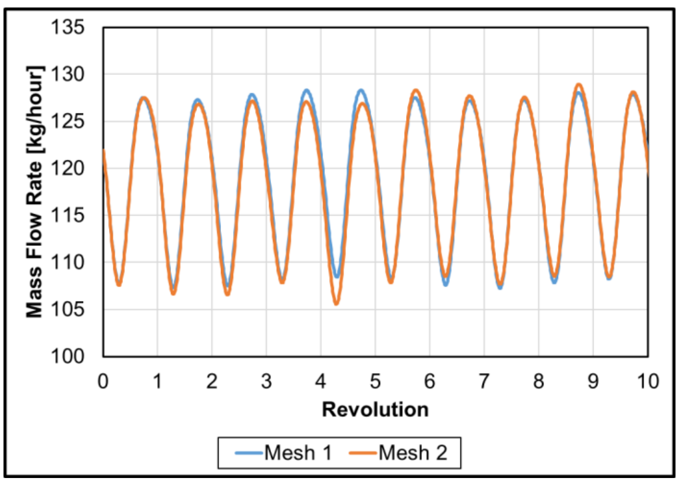

Figure 3: Comparison of mass flow rate through outlet boundary between cases with different mesh settings.

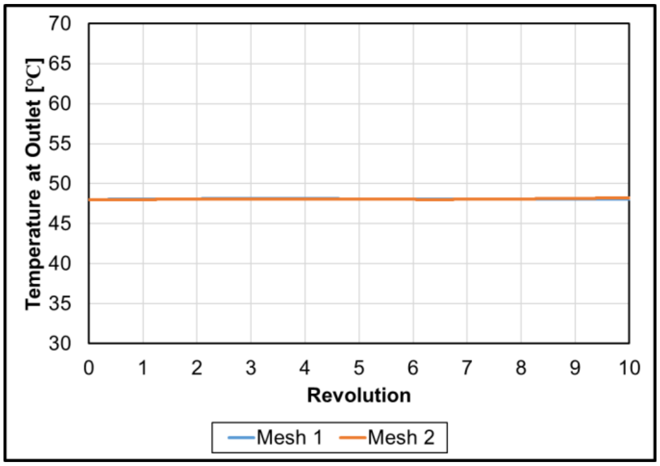

Figure 4: Comparison of temperature at outlet boundary between cases with different mesh settings.

3.2 Effect of Tip Leakage Size

Simulations were performed to study the effect of different tip leakage sizes ranging from 0 to 100 μm. A same tip leakage size is assumed on fixed and orbiting scroll sides. Figure 5 shows how the tip leakage is applied. Detailed information of cases with different tip leakage sizes are included in Table 2. Multiple compressor output variables are compared, including volumetric efficiency of E-Compressor and thermal properties in the downstream of E-Compressor.

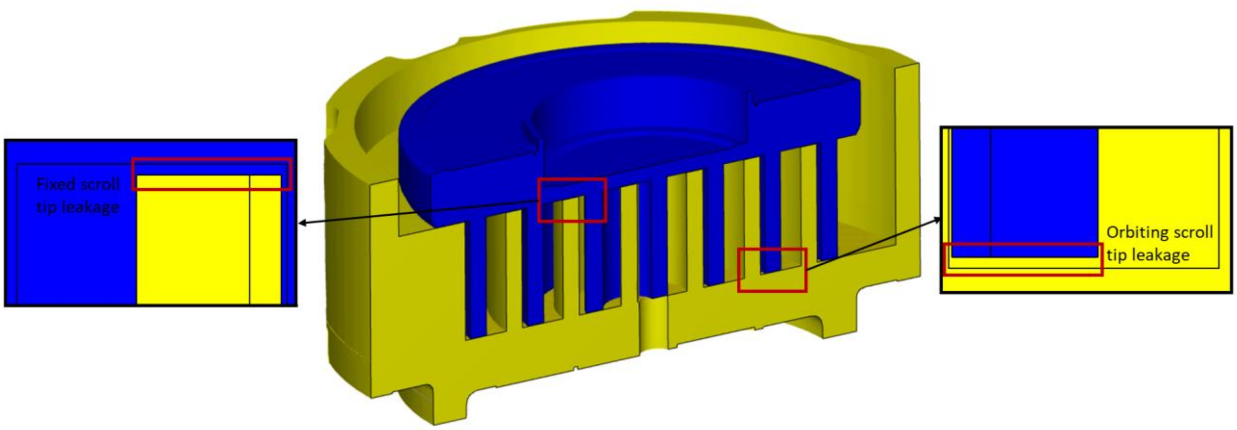

Figure 5: Tip leakage (enlarged for viewing) between the fixed (yellow) and orbiting scroll (blue).

Table 2: Case information with different tip leakage sizes

Case	Tip Leakage Size [μm]	Orbiting scroll side [μm]	Fixed scroll side [μm]
1	0	0	0
2	20	10	10
3	40	20	20
4	60	30	30
5	80	40	40
6	100	50	50

Figure 6 shows the outlet mass flow rate at the discharge port of the scroll compressor over a period of one revolution for different tip leakages. The maximum flow rate is observed close to crank angle of 115 degrees for all tip leakage sizes, but the flow output reduces as the tip leakage increases. The net flow rate across the compressor also reduces with increasing tip leakage size which leads to reduction of volumetric efficiency as shown in Figure 7. The volumetric efficiency is close to 96% for the case without any tip leakage and reduces up to 70% for the case with 100 μm tip leakage.

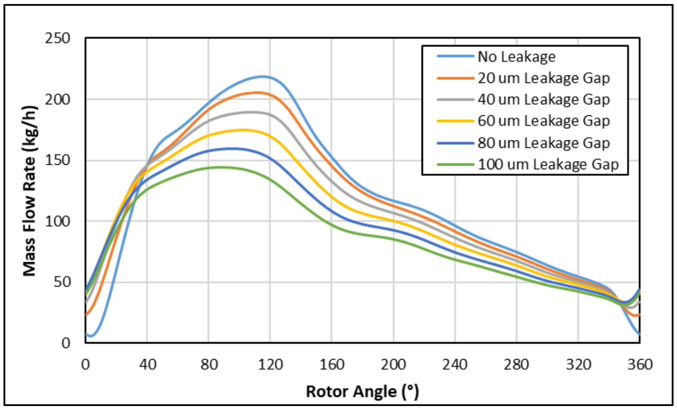

Figure 6: Outlet mass flow rate at discharge port of scroll compressor.

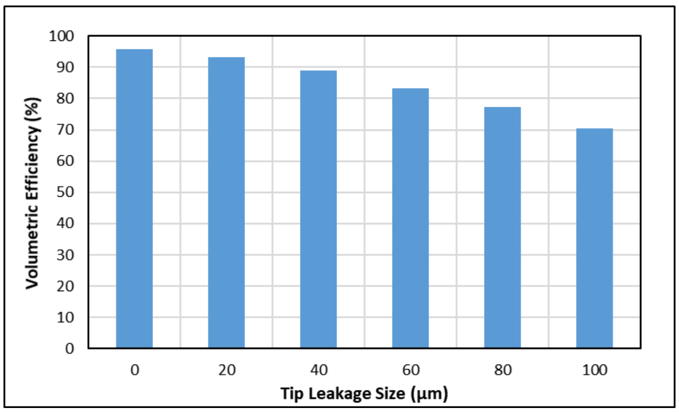

Figure 7: Volumetric Efficiency for different tip leakage sizes

The temperature output at the outlet boundary of the assembly is shown in Figure 8. The outlet temperature increases with tip leakage. There could be two reasons for this. Since the flow rate reduces with increasing tip leakage, the heat generated in the motor solids is not effectively cooled. This leads to higher temperatures for the motor coil, stator and rotor as shown in Figure 9. Subsequently, the fluid side temperatures are also higher. This leads to compression of high temperature fluid in the scroll compressor. The other reason could be higher residual time for fluid inside the compressor volume causing re-compression of high temperature refrigerant that leaks out of the tip leakage gaps into the suction side of the scroll compressor. Because of higher fluid side temperatures, the scroll solid temperatures also increase with tip leakage size as shown in Figure 10.

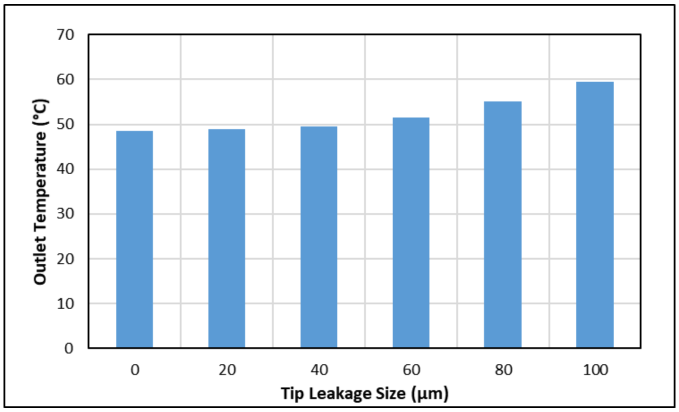

Figure 8: Temperature at outlet boundary of E-compressor for different tip leakage sizes

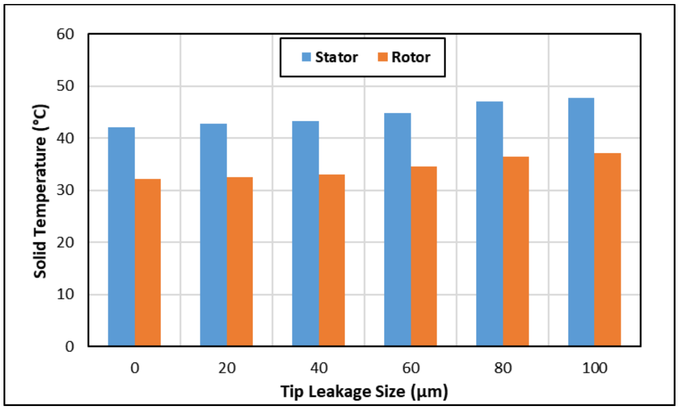

Figure 9: Maximum Solid Temperature in motor solids for different tip leakage sizes

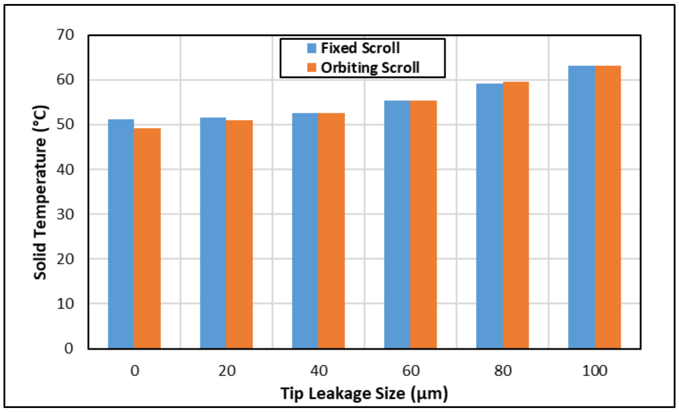

Figure 10: Maximum Solid Temperature in scroll solids for different tip leakage sizes

The temperature distribution on a cross section across the scroll compressor fluid is shown in Figure 11 for the Case 1 without any tip leakage. The temperature on the suction side is close to 23 °C and gradually increases as we move closer to the center. The temperature increases up to 57 °C. The temperature distribution on the solid E-compressor is shown in Figure 12. Higher temperatures are observed towards the bottom since the scroll compressor, that has the highest temperatures, is present near the bottom. The scroll solid temperatures are shown in Figure 13. The maximum temperature observed for the orbiting scroll is 50 °C while that for the fixed scroll is 51 °C. Maximum temperatures were observed near the center tip of the solids which correspond to the highest fluid temperature zones. Similar distribution was observed for other tip leakage gaps but with higher temperatures.

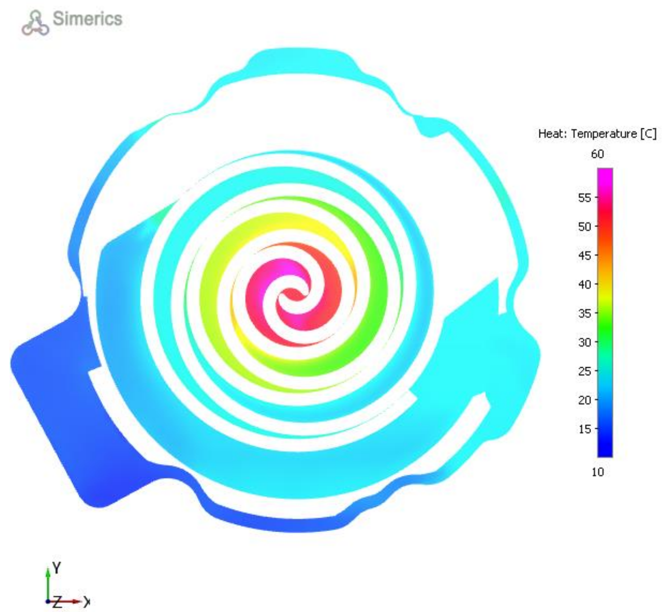

Figure 11: Temperature contours on mid-cross section through scroll fluid side for Case 1

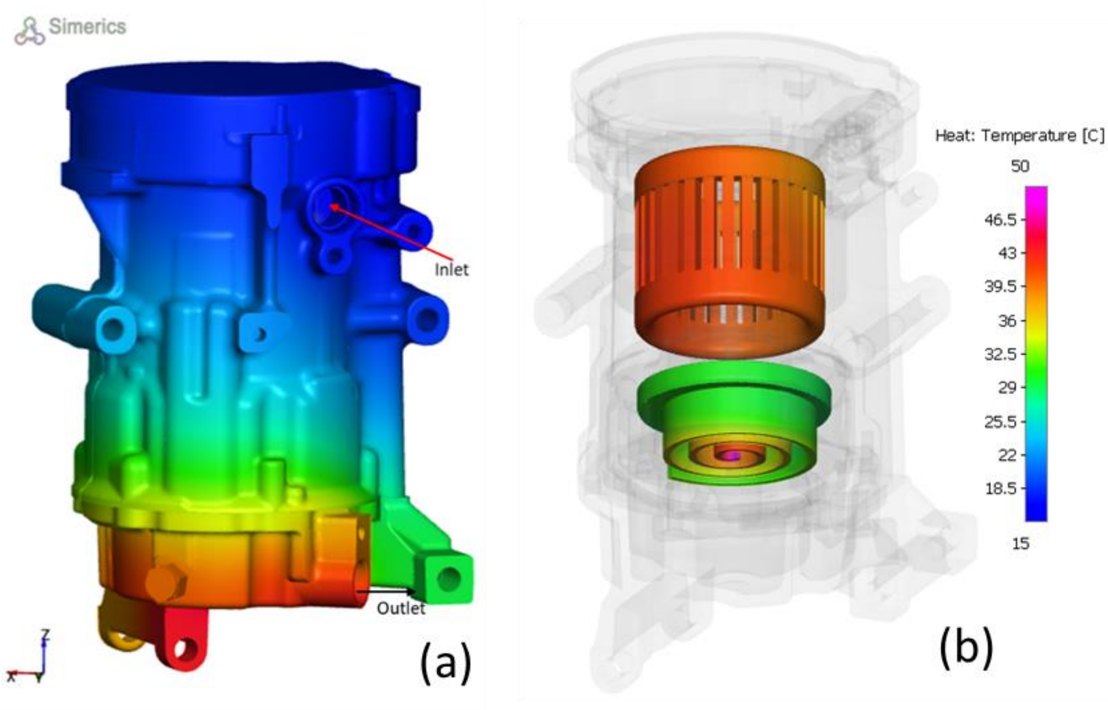

Figure 12: Temperature contours on the E-compressor (a) casing, (b) coil and orbiting scroll for Case 1

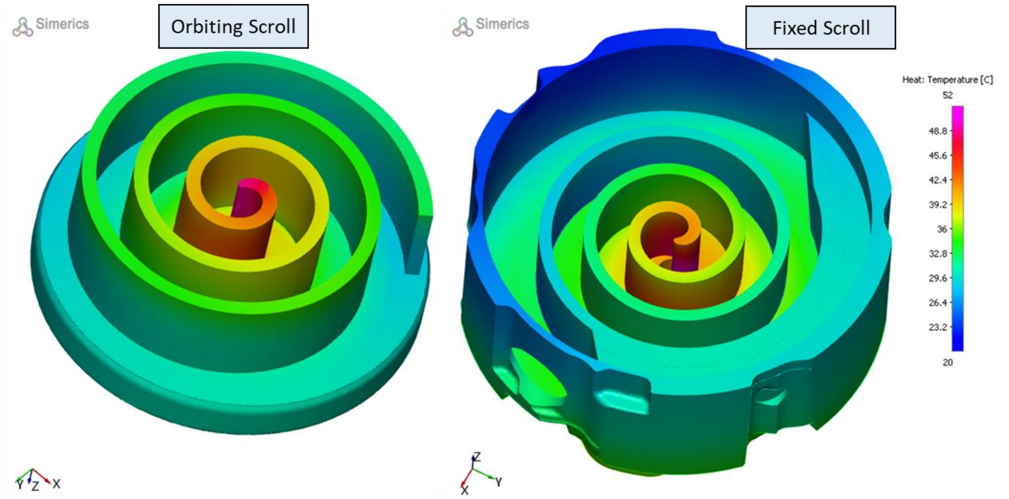

Figure 13: Temperature contours on fixed and orbiting scroll for Case 1

3.3 Effect of Reed Valve

A second set of simulations are performed where a reed valve is placed at the discharge port of the scroll compressor in order to study the influence of such valves on the compressor performance. Figure 14 shows the outlet flow rate at the discharge port for Case 1 without tip leakage over a period of one rotation of the orbiting scroll. It can be observed that with the reed valve, the discharge takes place in three parts over a period of a cycle instead of one wave observed in the case without reed valve, which indicates that the reed valve flutters thrice in one cycle. Also, the discharge flow rate reduces with each flutter as some fluid discharges after each flutter.

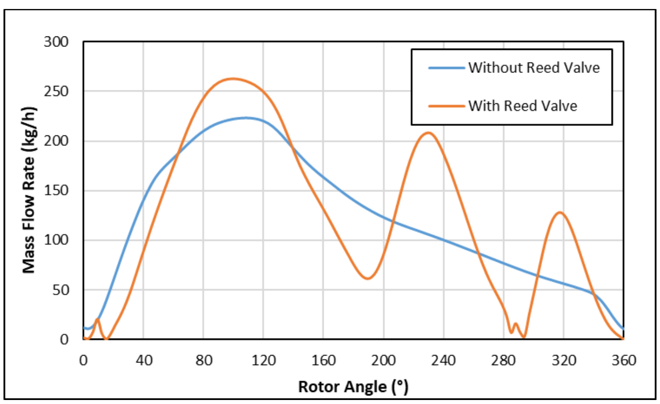

Figure 14: Outlet mass flow rate at discharge port of scroll compressor for Case 1

The opening of the reed valve is shown in Figure 15 for Case 1 and Case 3. The reed valve flutters three times in one cycle. Once sufficient pressure is built up in the scroll discharge chamber, the reed valve opens and discharges some fluid that leads to drop in pressure in the chamber and some closure of the reed valve. But the compression of the fluid continues, and the reed valve opens again but with a smaller angle. The same phenomenon is repeated for a third time with a smaller angle of opening. It is also observed that the opening of reed valve reduces with increasing tip leakage size.

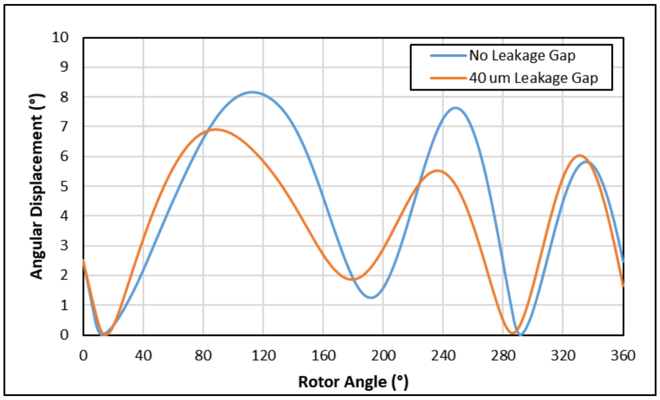

Figure 15: Reed valve opening over a period of cycle

Figure 16 shows the volumetric efficiency for different cases. Apart from reduction in volumetric efficiency due to tip leakage, there is further reduction due to the reed valve. This is because, when the reed valve is closed, more flow can leak through the tip leakage that leads to overall reduction of refrigerant flow.

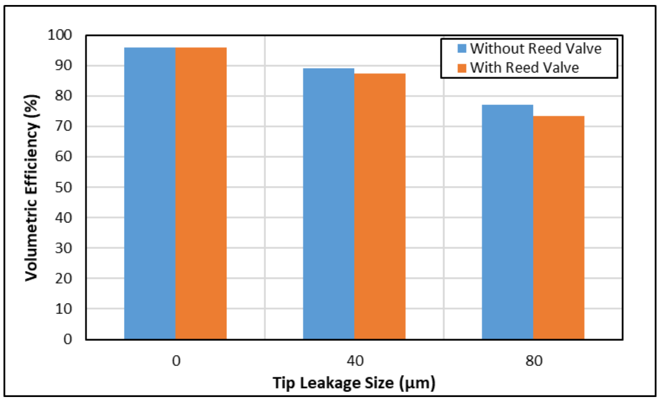

Figure 16: Volumetric Efficiency for different tip leakage sizes

Along with reduction in fluid flow rate and increased leakage flow, the overall fluid temperature also increases due to the reed valve as explained earlier. Figure 17 shows the outlet temperature for the E-compressor assembly with and without reed valve.

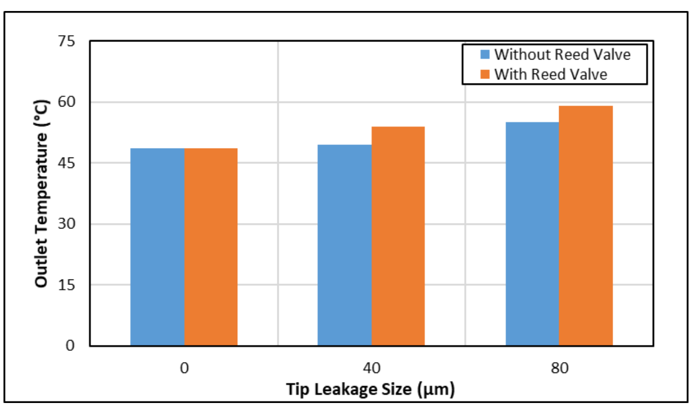

Figure 17: Temperature at outlet boundary of E-compressor for different tip leakage sizes

4. CONCLUSIONS

In the present work, the methodology for the 3D Conjugate Heat Transfer simulation of a scroll E-compressor using a commercial CFD program, SimericsMP+®, is shown. The simulation of both fluid and solids sides of the E-compressor is performed. The meshing of the scroll compressor was done using an automated template mesher that can also handle the strong deformation of the fluid regions. Using a Mixed Timescale Coupling approach, the simulations are performed to study the influence of axial leakage gaps on the performance of the scroll compressors. By including the solid thermal simulation also, the heat transfer is captured and affects inlet temperature of the fluid in the scroll compressor and in turn, its performance. Later, a reed valve is included at the discharge port of the scroll compressor to study its influence on the compressor performance. It is observed that axial leakage gaps and reed valve have a negative influence on the performance of scroll compressors. The developed methodology can be extended to perform parametric studies like the influence of different refrigerant inlet temperatures, operating pressures, ambient temperatures, etc. Using the template mesh for the scroll compressor and the circumferential valve makes the simulation setup easy and fast. Also, 2 cycles of the coupled simulation can be run in an hour on 64 cores that indicates a good computational efficiency.

References

Chen Y., Halm N.P., Groll E.A., Braun J.E. (2002), Mathematical modeling of scroll compressors—Part II: Overall scroll compressor modeling, *Int. J. Refrig. 25*, 751–764.

Cuevas C., Lebrun J. (2009), Testing and modelling of a variable speed scroll compressor, *Appl. Therm. Eng., 29*, 469-478.

Dhar, S., Godavarthi, R., Mishra, A., Bedekar, S. et al. (2019), A Transient, 3-Dimensional Multiphase CFD/Heat Transfer and Experimental Study of Oil Jet Cooled Engine Pistons, *SAE Technical Paper* 2019-01-0154.

Ding, H. and Gao, H. (2014), 3-D Transient CFD Model For A Rolling Piston Compressor With A Dynamic Reed Valve. *International Compressor Engineering Conference*.

Ding, H., Jiang, Y. & Dhar, S. (2019), CFD Modelling of Coupled Heat Transfer between Solid and Fluid in a Twin Screw Compressor. *IOP Conference Series: Materials Science and Engineering*.

Ding, H., Visser, F.C., Jiang, Y., and Furmanczyk, M. (2011), Demonstration and Validation of a 3D CFD Simulation Tool Predicting Pump Performance and Cavitation for Industrial Applications. *Journal of Fluids Engineering* 133.

Gao, H., Ding, H. & Jiang, Y. (2015), 3D Transient CFD Simulation of Scroll Compressors with the Tip Seal. *IOP Conference Series: Materials Science and Engineering*.

Gao, H. and Jiang, Y. (2014), Numerical Simulation of Unsteady Flow in a Scroll Compressor. *International Compressor Engineering Conference*. Paper 2337.

Lemmon, E., Huber, M. and McLinden, M. (2007), NIST Standard Reference Database 23: Reference Fluid Thermodynamic and Transport Properties-REFPROP, Version 8.0, Natl Std. Ref. Data Series (NIST NSRDS), National Institute of Standards and Technology, Gaithersburg, MD

Sun, S., Wu, K., Guo, P., Yan, J. (2017), Analysis of the three-dimensional transient flow in a scroll refrigeration compressor. *Applied Thermal Engineering*